Applied Clay Science 104 (2015) 252–260

Contents lists available at ScienceDirect

Applied Clay Science

journal homepage: www.elsevier.com/locate/clay

Research paper

Effective phosphate adsorption by Zr/Al-pillared montmorillonite: insight into equilibrium, kinetics and thermodynamics

Weiya Huang [a,b], Jie Chen [a], Fei He [a], Jinpeng Tang [a], Dan Li [c,*], Yi Zhu [a,**], Yuanming Zhang [a]

[a] Department of Chemistry, Jinan University, Guangzhou, 510632, China
[b] Department of Materials Science and Engineering, Taizhou University, Jiaojiang, 318000, China
[c] Chemical and Metallurgical Engineering and Chemistry, School of Engineering and Information Technology, Murdoch University, Murdoch, Western Australia, 6150, Australia

ARTICLE INFO

Article history:
Received 6 October 2014
Received in revised form 27 November 2014
Accepted 1 December 2014
Available online 19 December 2014

Keywords:
Pillared montmorillonite
Adsorption
Phosphate
Kinetics
Thermodynamics
Isotherms

ABSTRACT

Zirconium-pillared montmorillonite (Zr-Mt) and zirconium/aluminum-pillared montmorillonite (Zr/Al-Mt) were prepared by intercalating Zr^{4+} and Zr^{4+}/Al^{3+} polyhydroxy-cations into the interlayer spaces of natural montmorillonite (Mt). Zr-Mt and Zr/Al-Mt exhibited greater specific surface areas and pore volumes, as compared with Mt. In particular, the enhancement in the phosphate removal performance of Zr/Al-Mt was more significant in terms of phosphate adsorption capacity and rate, in relation to Zr-Mt. Herein, several important parameters, such as contact time, temperature, initial solution pH and competing anion, were investigated in detail to evaluate the phosphate adsorption performances of Zr/Al-Mt. The pseudo-second-order kinetic model fitted our acquired phosphate adsorption data best, in comparison with the use of the pseudo-first-order or the pseudo-third-order kinetic model. The Langmuir model appeared to fit the adsorption process better than that of the Freundlich model, with a maximum phosphate adsorption capacity of 17.2 mg P/g at 25 °C. The thermodynamic parameters (ΔG°, ΔH° and ΔS°) were also determined, which revealed that the phosphate adsorption process was spontaneous and endothermic in nature. A high adsorption capacity was observed at pH = 3.0, which decreased by increasing pH. The presence of competitive ions, e.g. Cl^-, NO_3^-, and SO_4^{2-}, slightly impacted the phosphate adsorption; whereas the introduction of CO_3^{2-} caused the greatest adverse effect. The study on the Zr/Al-Mt leaching strongly suggested that the risk of Zr^{4+} leakage during adsorption process be negligible within a wide pH range of 3.0–9.0. After three adsorption-desorption cycles, there was no significant loss in the adsorption performance of Zr/Al-Mt.

1. Introduction

Phosphate is an essential element to support the growth of most biological organisms in aquatic environment. However, the excessive amount of phosphate in water bodies induces eutrophication, which accelerates multiplication of algae, depletes dissolved oxygen, deteriorates water quality, and depopulates aquatic animals (Ye et al., 2006). Numerous approaches have been developed to treat phosphorus-rich effluent before its discharge into the natural water bodies, including *via* chemical precipitation, crystallization, ion exchange, adsorption, reverse osmosis and biological methods (Morse et al., 1998; de Bashan and Bashan, 2004; Grzmil and Wronkowski, 2006). Among them, adsorption is usually recommended as one of the most effective techniques, due to its suitability for technologically economical and highly efficient removal even of phosphate traces from water (Morse et al., 1998; Biswas et al., 2008; Awual et al., 2011; Ren et al., 2011).

Metal oxides/hydroxides, such as aluminum oxide (Genz et al., 2004), aluminum hydroxide (Tanada et al., 2003), zirconium oxide (Liu et al., 2008), zirconium hydroxide (Chitrakar et al., 2006), Fe-Zr binary oxide (Long et al., 2011), crystalline manganese oxide (Mustafa et al., 2006), Zn-Al-Zr ternary layered double hydroxide (Koilraj and Kannan, 2010) have been reported as highly efficient adsorbents in removing phosphate from aqueous media. However, it is not cost-effective utilizing pure metal oxides/hydroxides for practical phosphate removal. On the other side, clay minerals have been well known as abundant and low-cost materials, which show great potential for use as adsorbents. One of their drawbacks is the adsorption performance, including rate and capacity, far from satisfactory; thus a great deal of research effort has contributed to improvement. Recently, some particular research interest has been directed on the modification of clay minerals by using inorganic metal polyhydroxy-cations to replace the original cations in the clay minerals (Prasad et al., 2000; Babel and Kurniawan, 2003; Gimenez et al., 2007). The prepared materials, termed pillared interlayered clay minerals (or pillared clay minerals), can achieve both cost efficiency and high adsorption capacity (Biswas et al., 2008). Many of these metal-pillared clay minerals have been shown to be promising adsorbents in removing phosphate from water. For example,

* Corresponding author. Tel.: +61 8 93602569.
** Corresponding author. Tel.: +86 20 85222756.
E-mail addresses: l.li@murdoch.edu.au (D. Li), tzhury@jnu.edu.cn (Y. Zhu).

http://dx.doi.org/10.1016/j.clay.2014.12.002
0169-1317/

Yan et al. found that the phosphate removal capacities of Al-pillared bentonite and Fe-pillared bentonite were 12.7 mg P/g (38.9 mg of phosphate/g) and 11.2 mg P/g (34.3 mg of phosphate/g), respectively; whilst the un-pillared adsorbent could hardly adsorb phosphate from water (Yan et al., 2010). Kasama et al. prepared a series of montmorillonite, beidellite, saponite, and fluor-tetrasilicic expandable mica pillared with Keggin ion-like Al clusters (Kasama et al., 2004). Their maximum phosphorus adsorption capacities were 20.5 mg P/g (62.8 mg of phosphate/g), 24.5 mg P/g (75.1 mg of phosphate/g), 25.1 mg P/g (76.9 mg of phosphate/g), and 27.0 mg P/g (82.7 mg of phosphate/g), respectively, in contrast to undetectable phosphate adsorption capacities onto their parent clay minerals. Moreover, previous studies have reported the mixed metal-pillared clay minerals possessed superior phosphate adsorption capacities to the single metal-pillared ones (Tian et al., 2009; Zhou et al., 2010). For instance, the mixed La/Al-pillared montmorillonite was reported with an improved phosphate adsorption ability, which was approximately 1.3 times higher than that of Al-pillared montmorillonite (Tian et al., 2009).

Montmorillonite (Mt), a typical 2:1 cationic layered silicate clay mineral, is one of the most abundant clay minerals on the earth surface, with attractive characteristics of low cost and easy availability. A variety of pillared Mt, such as Fe/Zr, Ti, Al, and Zr, have been explored as efficient adsorbents to remove various pollutants, *i.e.* Cr(VI), arsenic and dyes, from water (Na et al., 2010; Gil et al., 2011). Particularly, previous studies have proven that Zr^{4+} active sites have remarkable selectivity to phosphorus; thus Zr^{4+}-containing adsorbents own high phosphate adsorption capacities and in turn great practical application potential (Chitrakar et al., 2006; Koilraj and Kannan, 2010; Long et al., 2011; Rodrigues et al., 2012). However, according to our literature survey, there have been no studies reported on the use of single Zr-pillared or its mixed metal-pillared Mt as the adsorbents in removing phosphate so far.

The aim of this work was, therefore, to explore the feasibility of Zr-pillared Mt (Zr-Mt) for phosphate adsorption; in particular, in order to further improve the adsorption ability, the mixed metal Zr/Al-pillared Mt (Zr/Al-Mt) was synthesized. Moreover, the phosphate adsorption equilibrium, kinetics and thermodynamics by utilizing our synthesized adsorbents, as well as the influences of other factors, including pH, temperature and competing anion, on the phosphate removal were detailed in this paper.

2. Materials and methods

2.1. Materials

The Mt used in this study was obtained from Minghui Mining Co. (Anhui, China) and used without any pretreatment. Zirconium (IV) oxychloride ($ZrOCl_2 \cdot 8H_2O$) was purchased from Aladdin Chemistry Co., Ltd, China. Aluminum chloride ($AlCl_3 \cdot 6H_2O$), potassium dihydrogen phosphate (KH_2PO_4) and other chemicals used in this study, including NaOH, Na_2CO_3, Na_2SO_4, NaCl, and HCl (32%), were obtained from Guangzhou Chemical Co. China. All of the reagents were analytical grade and used as received.

2.2. Preparation of adsorbents

The sample of Zr-Mt was synthesized according to the literature (Toranzo et al., 1998). 8.0 g Mt was added to 240.0 mmol/L $ZrOCl_2$ aqueous solution under vigorous stirring to obtain a Zr^{4+}/Mt ratio of 3.0 mmol/g. The mixture was stirred at room temperature for 2 h, followed by 4 h aging. After that, the resulting dispersion was filtered, and washed repeatedly with deionized (DI) water until there was no chloride, verified by the $AgNO_3$ test. The solid was dried at 80 °C, ground to 125 mesh, and stored in a sealed bottle.

The sample of Zr/Al-Mt was prepared as follows: 4.8 g $AlCl_3 \cdot 6H_2O$ was dissolved in 50.0 mL 0.2 M NaOH solution and hydrolyzed at 60 °C to form a pillaring solution with a molar ratio of $OH^-/Al^{3+} = 2.0$. 6.5 g $ZrOCl_2 \cdot 8H_2O$ was dissolved in 200.0 mL H_2O to obtain Zr^{4+}-solution. 8.0 g Mt was added into Zr^{4+}-solution to form a uniform mixture, in which the above Al^{3+}-pillaring solution was slowly added under stirring to obtain a dispersion with a Zr^{4+}/Al^{3+} molar ratio of 1. The resulting dispersion was stirred for 4 h at room temperature and then aged for 24 h, before it was filtered and washed repeatedly with DI water until there was no chloride. The solid was dried at 80 °C, ground to 125 mesh, and stored in a sealed bottle before use.

2.3. Characterization of adsorbents

X-ray diffraction (XRD) patterns were recorded on a Rigaku Dmax-RB diffractometer using CuKα radiation of 40 kV and 20 mA with the wavelength of 0.154 nm. The basal spacing of the sample was calculated by using Bragg equation $n\lambda = 2d \sin\theta$ from the position of the 001 reflection. Nitrogen adsorption-desorption isotherms were measured at 77 K using ASAP 2010 (Micromeritics Inc., USA). The BET specific surface area (SSA) was determined from the linear part of the BET plot ($P/P_0 =$ 0.05-0.20). The pore size was calculated from the adsorption branch of isotherm by using Barrett-Joyner-Hallenda (BJH). The total pore volume was evaluated from the adsorbed nitrogen amount at a relative pressure of 0.98. Surface morphology of the sample was examined by scanning electron microscopy (SEM, Philips XL-30, Eindhoven, Netherlands). The zeta potential of the Mt or Zr/Al-Mt dispersion (2 g/L) of different pH values was measured by a Zetasizer Nano ZS (Malvern Instruments, UK). The concentration of Zr^{4+} was determined by inductively coupled plasma atomic emission spectrophotometry (ICP-AES, Optima™ 2000 DV, PerkinElmer).

2.4. Batch adsorption experiment

A series of batch tests were conducted to investigate the phosphate adsorption performances of our adsorbents. The solution of phosphate was obtained by dissolving desired amount of KH_2PO_4 in DI water. Each of the experimental results was conducted three times and the average value was used. The concentration of phosphate was analyzed by Autoanalyzer 3 (Bran and Luebbe Inc., Germany) and expressed as mg P/L in this study (1 mg P/L = 3.06 mg of phosphate/L). Consequently, the adsorption capacity of the adsorbent was shown in mg P/g (1 mg P/g = 3.06 mg of phosphate/g).

2.4.1. Kinetic study

In kinetic studies, 0.2 g of each adsorbent was added into a conical flask with 100.0 mL of 40.0 mg P/L phosphate solution, where the pH values were adjusted to 5.0. The sealed flasks were then put in a shaker bath at 25 °C and shaken at 170 rpm for 480 min. 2.0 mL of dispersion was taken out over a given period of time and filtered through a syringe nylon-membrane filter (pore size 0.45 μm; Shanghai Minglie Science Technology Co. Ltd). Finally, the concentration of phosphate in filtrate was analyzed, and the amount of phosphate adsorbed onto the sample at different periods (q_t) was calculated by Eq. (1),

$$q_t = \frac{(C_0 - C_t) \times V}{m} \quad (1)$$

where C_0 and C_t were the phosphate concentrations in solution at initial and different time periods (mg P/L), respectively; V was the volume of solution (L) and m was the mass of adsorbent (g).

In order to model the kinetics of the adsorption process, the experimental data were fitted in the pseudo-first-order, pseudo-second-order, and pseudo-third-order models, which were described as Eqs. (2), (3) and (4) (Lagergren, 1898; Cheung et al., 2001; Ho, 2006):

$$\text{Pseudo-first-order kinetic model}: C_t = C_0 - (C_0 - C_e)\left(1 - e^{-k_1 t}\right) \quad (2)$$

$$\text{Pseudo-second-order kinetic model}: C_t = C_0-(C_0-C_e)\left(1-\frac{1}{1+k_2t}\right) \quad (3)$$

$$\text{Pseudo-third-order kinetic model}: C_t = C_0-(C_0-C_e)\left[1-\frac{1}{(1+2k_3t)^{1/2}}\right] \quad (4)$$

where t was the adsorption time (min); k_1 (1/min), k_2 (1/min), and k_3 (1/min) were the adsorption rate constants of the pseudo-first-order model, the pseudo-second-order model and the pseudo-third-order model, respectively.

2.4.2. Isotherm study

For the adsorption tests, 0.2 g of the adsorbent was added into a series of conical flasks with 100.0 mL phosphate solutions of various initial concentrations (20.0–50.0 mg P/L). The sealed flasks were then put in a shaker bath shaken at 170 rpm and at different temperatures (25 °C, 30 °C, and 35 °C) for 24 h. Afterwards, the dispersion was filtered through a 0.45 μm membrane filter and the filtrate was analyzed for phosphate concentration. The equilibrium adsorption capacity was calculated by Eq. (5),

$$q_e = \frac{(C_0-C_e)\times V}{m} \quad (5)$$

where C_0 and C_e were the initial and equilibrium phosphate concentrations in solution (mg P/L), respectively; V was the volume of solution (L) and m was the mass of adsorbent (g).

The equilibrium data were fitted to the well-known Langmuir and Freundlich isotherm models, as shown in Eqs. (6) and (7), respectively (Langmuir, 1917; Freundlich, 1906):

$$\text{Langmuir model}: q_e = q_m K_L \frac{C_e}{1+K_L C_e} \quad (6)$$

$$\text{Freundlich model}: q_e = K_F C_e^{1/n} \quad (7)$$

where C_e (mg P/L) and q_e (mg P/g) were phosphate concentration and corresponding adsorption capacity at the equilibrium. q_m (mg P/g) was the maximum adsorption capacity and K_L was the Langmuir adsorption equilibrium constant, which were related to adsorption capacity and energy or net enthalpy of adsorption. K_F and n were the constants in the Freundlich isotherm model, which measured the adsorption capacity and intensity, respectively.

2.4.3. Thermodynamic study

Three fundamental thermodynamic parameters, *i.e.* ΔG°, ΔH° and ΔS°, were calculated to evaluate the thermodynamic feasibility and the nature of the adsorption process. ΔG° was calculated according to the following equation:

$$\Delta G^0 = -RT\ln K_d \quad (8)$$

where R was the gas constant, T was the temperature in Kelvin and K_d was the thermodynamic equilibrium constant of the adsorption process, reflecting phosphate distribution between the solid and liquid phases at equilibrium. K_d was determined by plotting $\ln(q_e/C_e)$ *vs.* q_e and extrapolating q_e to zero (Khan and Singh, 1987). ΔH° and ΔS° were evaluated using Van't Hoff equation as follows:

$$\ln K_d = \frac{\Delta S^0}{R} - \frac{\Delta H^0}{RT} \quad (9)$$

The slope and intercept of the linear plot of $\ln K_d$ *vs.* 1/T were used to determine the values of ΔH° and ΔS°.

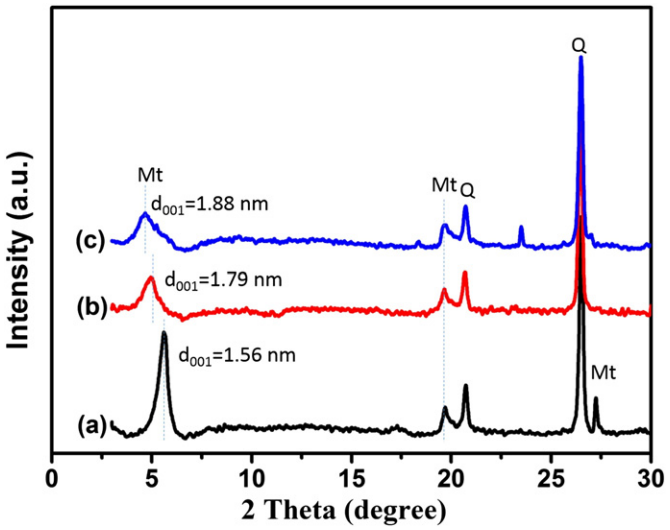

Fig. 1. X-ray diffraction patterns of Mt (a), Zr-Mt (b) and Zr/Al-Mt (c) (Q in Fig. 1 is referred to quartz).

2.4.4. Effects of initial pH and competing anions

To determine the effect of pH on phosphate adsorption, 0.2 g of the adsorbent was added into a series of 100.0 mL phosphate solution (40.0 mg P/L) of various initial pH values, ranging from 3.0 to 10.0. The initial pH of phosphate solution was adjusted with 1 M NaOH or 1 M HCl solution. To evaluate the effect of competing anions on phosphate adsorption, 0.2 g of the adsorbent was added into 100.0 mL of 40.0 mg P/L phosphate solutions containing 3.0 mmol/L competing anion, which was prepared by dissolving sodium salt form of CO_3^{2-}, Cl^-, SO_4^{2-}or NO_3^-. The resulting samples were placed in the shaker bath for 24 h, and the phosphate concentration in solution was determined as described above.

2.4.5. Zr^{4+} leaching experiment

To evaluate the Zr^{4+} leaching in the adsorbent during phosphate adsorption, 0.2 g of the sample was added to 100.0 mL of 40.0 mg P/L phosphate solution with desired pH values, and the mixture was shaken for 24 h at 25 °C. After that, the dispersion was filtered and the desorbed Zr^{4+} in the filtrate was analyzed by ICP-AES.

2.4.6. Adsorption-desorption cycles

The phosphate adsorption-desorption cycles were repeated three times to evaluate the reusability of our adsorbent. In the adsorption test, Zr/Al-Mt was treated in 40.0 mg P/L phosphate solution as described above to obtain phosphate-loaded adsorbent. In the desorption process, the spent adsorbent was immersed in 0.1 M NaOH solution, and shaken at room temperature for 24 h. The desorbed samples were separated by filtration, washed with DI water and dried at room temperature. Following that, the above regenerated adsorbent was reused for next-cycle.

Table 1
Structure characteristics of Mt, Zr-Mt, and Zr/Al-Mt.

Adsorbents	SSA (m^2/g)	Average pore diameter (nm)	Total pore volume (cm^3/g)
Mt	33.6	9.4	0.0008
Zr-Mt	163.4	2.7	0.06
Zr/Al-Mt	198.6	2.4	0.07

3. Results and discussion

3.1. Adsorbent characterization

The XRD patterns of Mt, Zr-Mt and Zr/Al-Mt are shown in Fig. 1. The raw Mt showed a characteristic reflection ($2\theta = 5.66°$) of the Mt crystalline structure, corresponding to the d_{001}-value of 1.56 nm (Fig. 1a). The reflections at 20.71° and 26.45° were corresponding to the quartz (denoted as Q), which was suggested to be present in Mt (Fig. 1a). The d_{001}-values of the samples Zr-Mt and Zr/Al-Mt were 1.79 nm and 1.88 nm, according to their reflections at 4.75° and 4.92° (Fig. 1b–c), respectively. Compared with Mt, the d_{001}-value of Zr/Al-Mt was increased by 0.32 nm, whilst that of Zr-Mt was increased by 0.23 nm. This reveals that the Zr^{4+} and Zr^{4+}/Al^{3+} polyhydroxy-cations were successfully intercalated into the interlayers of Mt. Moreover, both of the reflections in the pillared samples were slightly broader, compared to that of Mt. This may be caused by the differences in crystallinity after intercalating Zr^{4+} or Zr^{4+}/Al^{3+} polyhydroxy-cations into Mt (Guerra et al., 2008).

Table 1 summarizes the SSA, average pore diameters and total pore volumes of Mt, Zr-Mt and Zr/Al-Mt. The SSA and total pore volume of Zr/Al-Mt were 198.6 m^2/g and 0.07 cm^3/g; whilst those of Zr-Mt were 163.4 m^2/g and 0.06 cm^3/g, respectively. Obviously, the pillared samples showed significantly larger SSA and total pore volumes than those of Mt, indicating that Zr^{4+} or Zr^{4+}/Al^{3+} polyhydroxy-cations were successfully intercalated into Mt, in accordance with the XRD observations (Fig. 1). Meanwhile, coupled with significant increase of SSA and total pore volumes, the average pore diameters for both samples decreased after pillaring; these could probably be attributed to the formation of new micropores during the pillaring process (Zhou et al., 2010).

SEM images of Mt, Zr-Mt and Zr/Al-Mt are shown in Fig. 2. Mt appeared in block-like crystals (Fig. 2a), with lamellar surfaces at high magnification (Fig. 2b). The prepared Zr-Mt (Fig. 2c) and Zr/Al-Mt

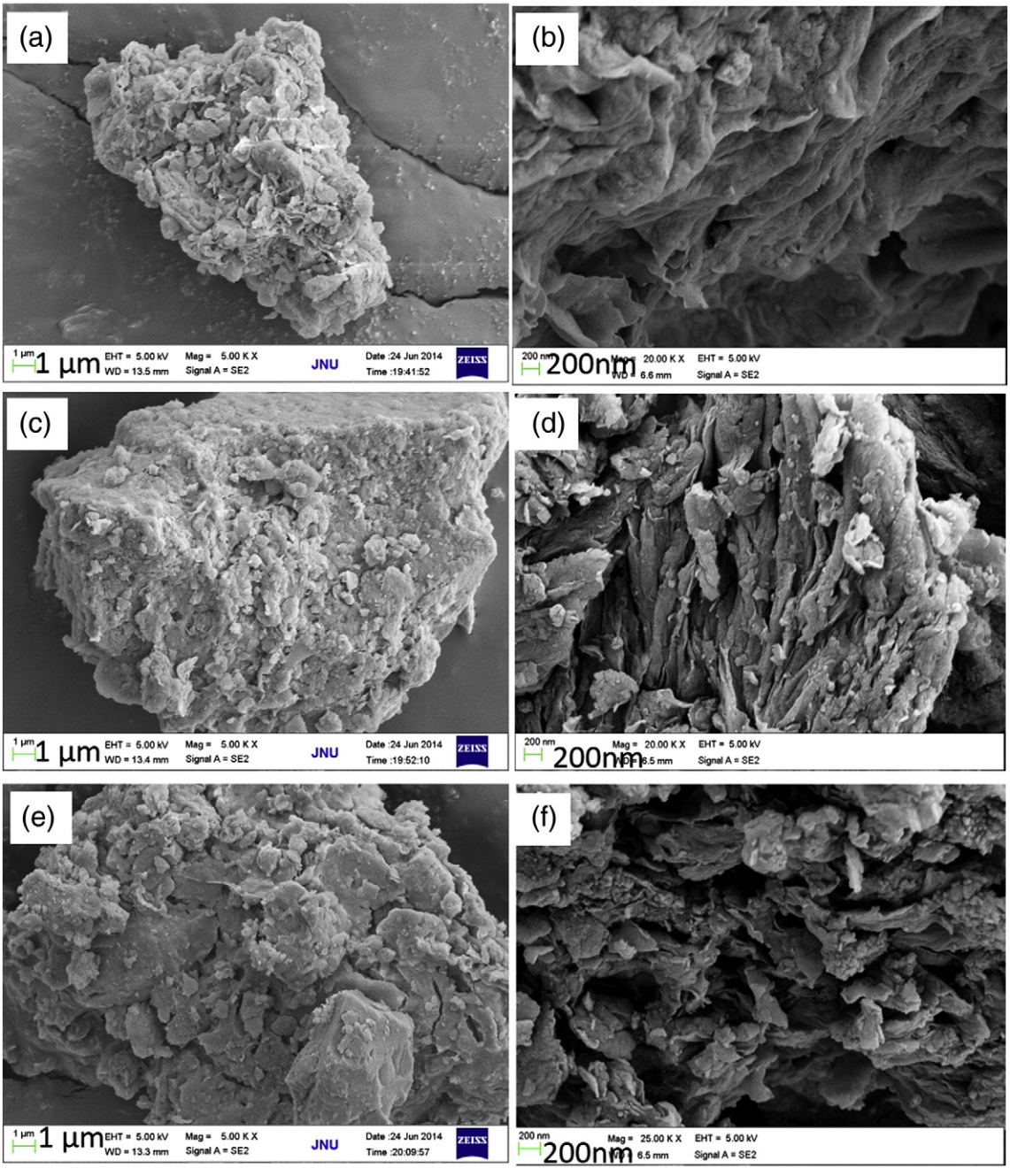

Fig. 2. SEM images of Mt (a and b), Zr-Mt (c and d) and Zr/Al-Mt (e and f).

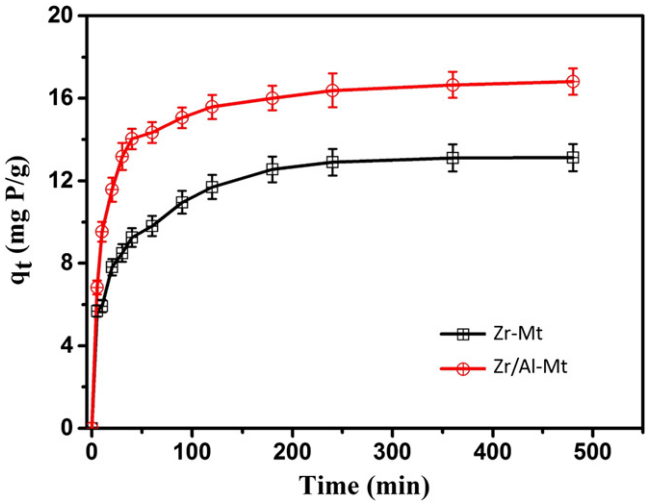

Fig. 3. Effect of contact time on the adsorption capacities of Zr-Mt and Zr/Al-Mt.

(Fig. 2e) exhibited similarly block-like particles; however, the surface morphology (Fig. 2d and f) slightly differed, that was the samples after the pillaring process presenting in the foliated stage with a number of lamellas formed in a stacking structure. In addition, the pillared samples became rougher with some small foliated flakes observed on their surfaces, which may contribute to the larger SSA as compared to Mt (Table 1).

3.2. Adsorption kinetics

The phosphate adsorption capacity of the samples as a function of adsorption time is shown in Fig. 3. For comparison, the adsorption experiment by using the parent Mt was carried out as well; that its adsorption capacity was zero over a period of 480 minutes. As can be seen in Fig. 3, the phosphate adsorption onto Zr/Al-Mt increased rapidly in the first 40 minutes and then changed gradually until q_t reached ~16.7 mg P/g after 360 min, where the adsorption equilibrium attained. A similar adsorption profile was observed with the use of the sample Zr-Mt, where the equilibrium was also achieved after 360 min. However, the equilibrium adsorption capacity of Zr-Mt was ~13.1 mg P/g, which was much lower than that of Zr/Al-Mt (~16.7 mg P/g); suggesting that the phosphate adsorption be greatly enhanced by utilizing the mixed metal-pillared Mt.

Table 2
Kinetic parameters for phosphate adsorption on Zr-Mt and Zr/Al-Mt.

Sample	Pseudo-first-order		Pseudo-second-order		Pseudo-third-order	
	k_1	R^2	k_2	R^2	k_3	R^2
Zr-Mt	0.0387	0.854	0.0775	0.961	0.164	0.955
Zr/Al-Mt	0.0642	0.925	0.123	0.997	0.272	0.972

The adsorption kinetics were further modelled using the pseudo-first-order, pseudo-second-order and pseudo-second-order models, as shown in Fig. 4; the corresponding parameters and correlation coefficients (R^2) are listed in Table 2. The results showed that the pseudo-second-order kinetic model fitted the experimental data best among these three models, with $R^2 = 0.997$ for the sample Zr/Al-Mt and $R^2 = 0.961$ for the sample Zr-Mt; suggesting that the phosphate adsorption onto Zr/Al-Mt and Zr-Mt be chemisorption (Ho et al., 2004). This is in a good agreement with the previous findings by using other phosphate adsorbents, including hydrous zirconium oxide (Rodrigues et al., 2012), magnetic Fe-Zr binary oxide (Long et al., 2011), and Zr-loaded orange waste gel (Biswas et al., 2008). Moreover, the rate constant k_2 derived from the pseudo-second-order fitting plot of Zr/Al-Mt was 0.123 min^{-1}, which was much greater than that of Zr-Mt, 0.0775 min^{-1}, indicating a faster adsorption of phosphate onto Zr/Al-Mt. Therefore, the sample Zr/Al-Mt exhibits dramatically

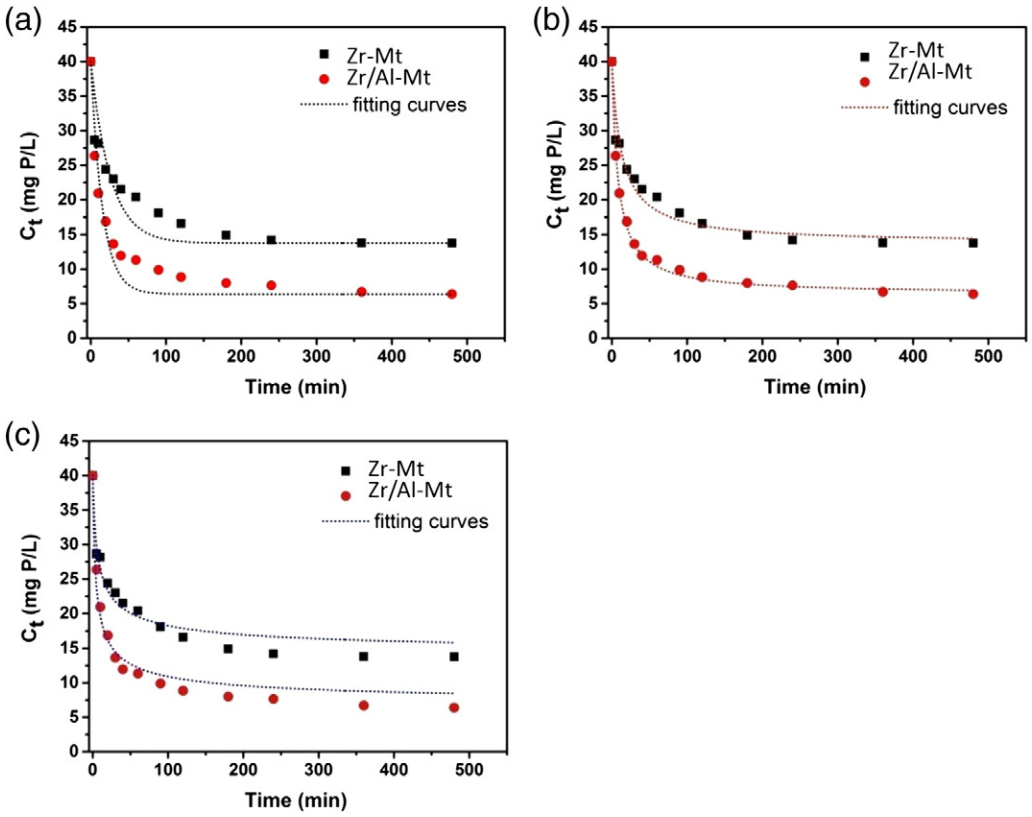

Fig. 4. (a) Pseudo-first-order, (b) pseudo-second-order and (c) pseudo-third-order fitting plots of the phosphate adsorption onto Zr-Mt and Zr/Al-Mt.

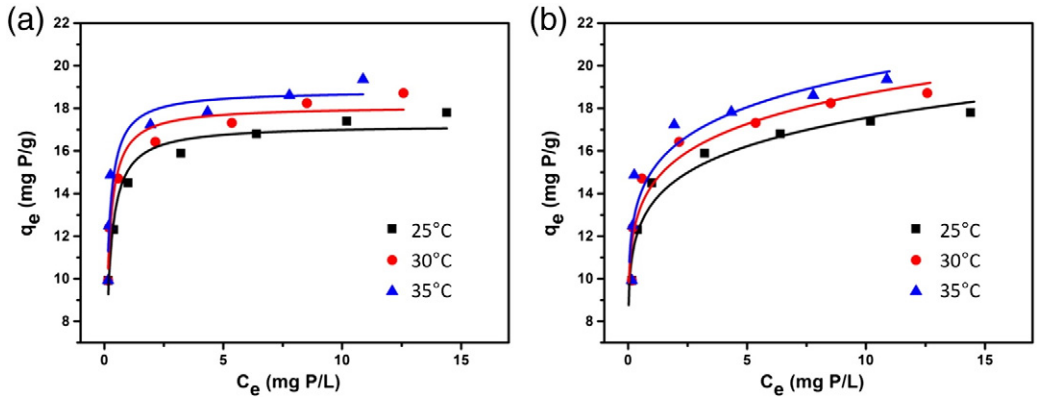

Fig. 5. (a) Langmuir and (b) Freundlich adsorption isotherms of Zr/Al-Mt at 25 °C, 30 °C, and 35 °C, respectively.

enhanced phosphate removal performance, including much higher phosphate adsorption capacity and faster adsorption rate, as compared with the sample Zr-Mt. Herein, Zr/Al-Mt was chosen in our further phosphate adsorption isotherm study.

3.3. Adsorption isotherms

Fig. 5 shows Langmuir (a) and Freundlich (b) adsorption isotherms of Zr/Al-Mt in the solution with various initial phosphate concentrations at 25 °C, 30 °C, and 35 °C. Table 3 summarizes the corresponding isotherm parameters and their correlation coefficients. In Table 3 and Fig. 5, high correlation coefficients ($R^2 > 0.916$) were derived by fitting experimental data into the Langmuir isotherm model, as compared with the Freundlich isotherm model ($R^2 > 0.844$). This suggests that the observed adsorption feature onto Zr/Al-Mt could be assigned to a monolayer coverage, which is in an agreement with the reported findings by utilizing other adsorbents, such as Fe-Zr binary oxide (Long et al., 2011; Ren et al., 2012), and La-modified bentonite (Haghseresht et al., 2009). In Table 3, the value of q_m at 25 °C was 17.2 mg P/g, which increased at higher temperature (Fig. 5). This suggests that the interaction between phosphate and the pillared adsorbent is endothermic in nature. Moreover, Zr/Al-Mt possesses a considerable adsorption capacity, compared to other single metal or mixed metal-modified clay mineral adsorbents in literature, as shown in Table 4.

3.4. Thermodynamics analysis

The values of thermodynamic parameters, *i.e.* ΔG°, ΔH° and ΔS°, are used to determine the spontaneous nature of the processes and provide essential information evaluating adsorbent practicability. Fig. 6 shows the linear plot of $\ln k_d$ *vs.* 1/T, and the obtained thermodynamic parameters are given in Table 5. The values of ΔG° obtained at all temperatures were negative, indicating that the adsorption of phosphate onto Zr/Al-Mt is a spontaneous and favorable process in nature. The decrease in ΔG° from −5.56 kJ/mol to −6.34 kJ/mol coupled with a rise in temperature from 25 °C to 35 °C implies the increase of spontaneity at higher temperatures. The positive value of ΔH° confirms the endothermic nature of adsorption. This is in accordance with the aforementioned result depicted by the isotherms (Fig. 5 and Table 3); that the adsorption capacity increased at higher temperature. The values of ΔS° were positive thus indicating a good affinity of phosphate ions towards the adsorbent and an increasing randomness at the solid–solution interface during the adsorption process. These results are consistent with the phosphate adsorption onto the $Ca(OH)_2$-bentonite (Ma et al., 2012), and the bentonites pillared with Fe^{3+} and Al^{3+} polyhydroxy-cations (Yan et al., 2010), in literature.

Table 3
Langmuir and Freundlich isotherm parameters for the phosphate adsorption onto Zr/Al-Mt at 25 °C, 30 °C and 35 °C.

Temperature (°C)	Langmuir			Freundlich		
	q_m (mg P/g)	K_L (L/mg P)	R^2	n	K_F	R^2
25	17.2	7.06	0.952	13.5	8.78	0.936
30	18.1	8.59	0.946	14.4	8.79	0.896
35	18.9	9.35	0.916	15.0	8.83	0.844

3.5. Effect of initial pH

The initial pH of the solution is an important variable influencing the adsorption of phosphate onto the adsorbents (Tanada et al., 2003; Ye et al., 2006; Huang et al., 2008); thus experiments were carried out here to examine the impact of initial pH affecting phosphate adsorption onto Zr/Al-Mt. The adsorption capacities of phosphate on Zr/Al-Mt as a function of pH values ranging from 3.0 to 10.0 are shown in Fig. 7a. A high adsorption capacity of 18.4 mg P/g was observed at pH = 3.0, while it dramatically dropped to 6.8 mg P/g at pH 10.0. Obviously, the adsorption of phosphate on the adsorbent was strongly pH-dependent: the adsorption capacity decreased with increasing initial pH value; this is similar to a number of reports using other Zr-containing adsorbents (Chitrakar et al., 2006; Zhang et al., 2013).

It is known that the phosphate can exist in different ionic species of $H_2PO_4^-$, HPO_4^{2-}, and PO_4^{3-}, depending on the pH of solution (pK_1 = 2.15, pK_2 = 7.20, and pK_3 = 12.33) (Perrin and Dempsey, 1979). Herein, when the pH value is between 3.0 and 7.20, the main species in solution is monovalent $H_2PO_4^-$; whilst in the pH between 7.20 and 10.0, the predominant species of phosphate is HPO_4^{2-}. Fig. 7b shows the effect of

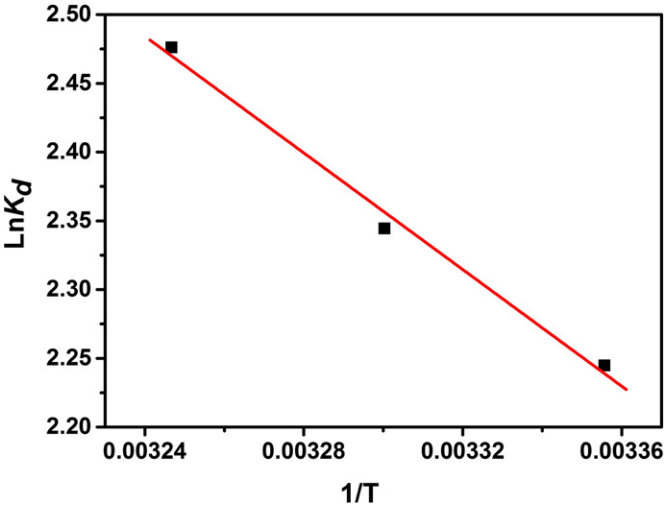

Fig. 6. Van't Hoff plot for the adsorption of phosphate by Zr/Al-Mt.

Table 4
Comparison of phosphate adsorption capacity of Zr/Al-Mt with other single metal or mixed metal-modified clay mineral adsorbents in literature.

Adsorbents	pH	Temperature (°C)	Adsorption capacity (q_m, mg P/g)	References
La-doped vesuvianite	7.1	/	6.7	Li et al. (2009)
Al-pillared bentonite	3.0	/	12.7	Yan et al. (2010)
Fe-pillared bentonite	3.0	/	11.2	Yan et al. (2010)
Al-pillared Mt	5.0	25	10.3	Tian et al. (2009)
La/Al-pillared Mt	5.0	25	13.0	Tian et al. (2009)
Zr/Al-Mt	5.0	25	17.2	Present work

pH on the zeta potential of Zr/Al-Mt. The isoelectric point pH_{zpc} of the Zr/Al-Mt was as high as 9.2, while the zeta potential values of raw montmorillonite were totally negative in the whole tested pH range. This indicated that positive charges were introduced into Mt by pillaring with Zr^{4+}/Al^{3+} polyhydroxy-cations. At the pH values less than 9.2, the surface of Zr/Al-Mt was protonated and showed positively charged; this favored the electrostatic attraction to phosphate species $H_2PO_4^-$ and HPO_4^{2-}. The decrease in phosphate adsorption with increasing pH values is ascribed from the change in surface charge which became less positive or even more negative at higher pH values. Besides, the competition between hydroxide groups and phosphate species for the adsorption sites could also account for the lower phosphate adsorption at higher pH values (Tian et al., 2009; Zhou et al., 2012).

On the other side, ligand exchange has been suggested as one of the possible mechanisms causing the change of phosphate adsorption onto the adsorbents in solution with different pHs in literature (Goldberg and Sposito, 1985; Tanada et al., 2003; Namasivayam and Prathap, 2005; Zhou et al., 2012). During the process of ligand exchange, hydroxyl group located on the adsorbent was replaced by phosphate and then released to the solution (shown in the following reactions), resulting in the increase of pH value. The change of solution pH during adsorption was closely monitored; our result showed that the pH of initial 40.0 mg P/L phosphate solution was 5.1 and slightly increased to 5.5 at final adsorption equilibrium with the use of Zr/Al-Mt. This would strongly confirm the ligand exchange process occurred during adsorption. However, we believe that the ligand exchange might not be the major mechanism governing the phosphate adsorption herein, since the increase of pH during the whole process is only 0.4.

$$M-OH + H_2PO_4^- \leftrightarrow M-(H_2PO_4) + OH^-$$
$$M-(OH)_2 + HPO_4^{2-} \leftrightarrow M-(HPO_4) + 2OH^-$$
$$M-(H_2PO_4) \rightarrow M-(HPO_4)^- + H^+$$
$$M-(HPO_4)^- + H_2O \leftrightarrow M-(H_2PO_4) + OH^-$$

3.6. Effect of competing anions

Many anions coexist with phosphate in water bodies and may compete with phosphate for the adsorption sites, thus interfering with the adsorption process. The impacts of several competing anions, *i.e.* SO_4^{2-}, NO_3^-, Cl^-, and CO_3^{2-}, on phosphate adsorption are shown in Fig. 8. In the presence of SO_4^{2-}, Cl^-, and NO_3^-, only slight decreases in adsorption capacities were observed. The phosphate adsorption capacities were reduced by 4.7%, 6.4%, and 8.1% with the presence of SO_4^{2-}, Cl^-, and NO_3^- respectively, indicating that these anions can hardly affect the strong adsorption of phosphate onto Zr/Al-Mt. By contrast, the addition of CO_3^{2-} greatly affected the adsorption capacity of phosphate onto Zr/Al-Mt, with a reduction of 25.0%. This is probably due to the basic nature of CO_3^{2-} increasing solution pH which might interfere with the equilibrium between HPO_4^{2-} and PO_4^{3-} as well as compete with phosphate for the adsorption active sites, thus lowering phosphate uptake more significantly (as shown in Fig. 7a). Our results show similarities with those for the phosphate adsorption onto other solid adsorbents, such as the Mt pillared with Al^{3+} or La^{3+}/Al^{3+} polyhydroxy-cations (Tian et al., 2009).

3.7. Zr^{4+} leaching

The risk of Zr^{4+} leakage from Zr/Al-Mt during adsorption is of importance in terms of its applicability in practical phosphate removal. The releasing behavior of Zr^{4+} was examined by measuring Zr^{4+} concentrations in the solution under different pH values (3.0–10.0), as shown in Fig. 9. Within the pH range of 3.0–9.0, the Zr^{4+} concentrations in the solutions were almost zero, indicating the good stability of the intercalated Zr^{4+} polyhydroxy-cations in the Zr/Al-Mt.

3.8. Adsorption-desorption cycles

Fig. 10 shows the phosphate adsorption capacities in cycles of adsorption-desorption. As can be seen, the phosphate adsorption

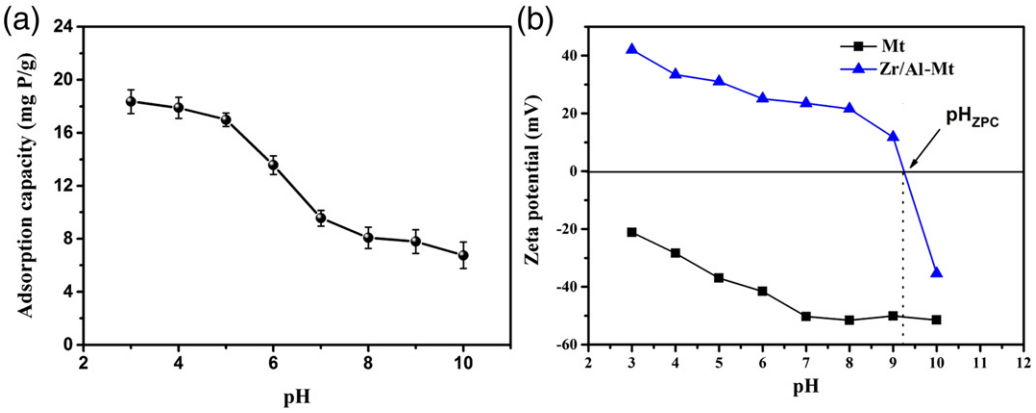

Fig. 7. (a) Effect of pH on the adsorption capacity of Zr/Al-Mt. (b) Effect of pH on the zeta potential of Zr/Al-Mt; that of raw Mt is also shown for comparison.

Table 5
Thermodynamic parameters for phosphate adsorption on Zr/Al-Mt at 25 °C, 30 °C, and 35 °C, respectively.

Temperature (°C)	K_d	△G° (kJ/mol)	△S°(J/mol K)	△H°(kJ/mol)
25	9.437	−5.56		
30	10.427	−5.91	77.79	17.64
35	11.893	−6.34		

capacity in the first adsorption-desorption cycle was 16.8 mg P/g, while the adsorption capacities in the second and third adsorption-desorption cycle were only decreased by 3.0% and 5.3%, as compared to the one in the first cycle. Obviously, the adsorbed phosphate ions in the spent adsorbent could be easily desorbed by using 0.1 M NaOH solution; and the sample Zr/Al-Mt possessed a superior regeneration capacity. This indicates that Zr/Al-Mt can be repeatedly used for phosphate removal without a significant loss in its adsorption performance.

4. Conclusions

Zr-Mt and Zr/Al-Mt were prepared for phosphate removal for the first time; and the sample Zr/Al-Mt exhibited significantly enhanced phosphate removal performances in the batch tests. The XRD results confirmed the successful introduction of Zr^{4+}/Al^{3+} polyhydroxy-cations into the interlayers of Mt with increasing basal spacing (d_{001}-value). The resulting Zr/Al-Mt exhibited larger SSA and total pore volume; as well as higher positive charges on external surfaces ($pH_{zpc} = 9.2$), which were believed to favor the adsorption of phosphate from water. The phosphate adsorption by Zr/Al-Mt obeyed the pseudo-second-order kinetic model best, suggesting it be chemisorption; while the adsorption isotherms followed the Langmuir model better than the Freundlich model. Its phosphate adsorption capacities increased with decreasing pH; accompanied with the zeta potentials of Zr/Al-Mt, this revealed the phosphate adsorption could likely be explained by electrostatic attraction. The presence of competing ions, *i.e.* SO_4^{2-}, Cl^-, and NO_3^-, only slightly affected adsorption capacities; whilst the introduction of CO_3^{2-} reduced the adsorption capacity by 25.0%. The risk of Zr^{4+} leakage was almost negligible in a wide pH range of 3.0–9.0; and the spent adsorbent could be regenerated and repeatedly used for phosphate removal without a significant loss in its adsorption performance. Our results suggested that Zr/Al-Mt be utilized as a potentially effective phosphate adsorbent for practical applications.

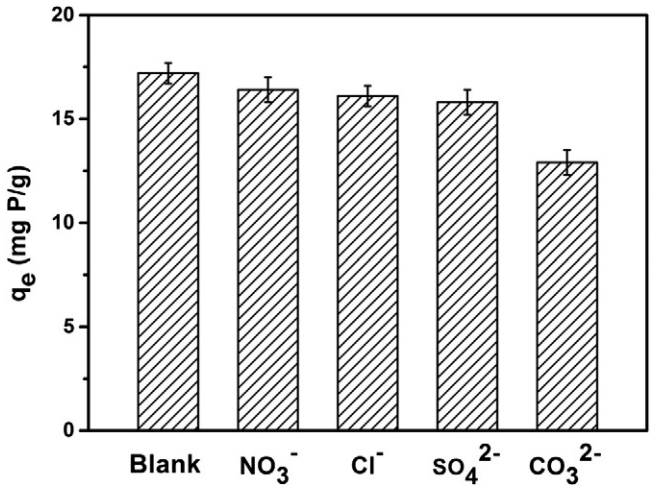

Fig. 8. Effect of competing anions on the phosphate adsorption capacity by using Zr/Al-Mt.

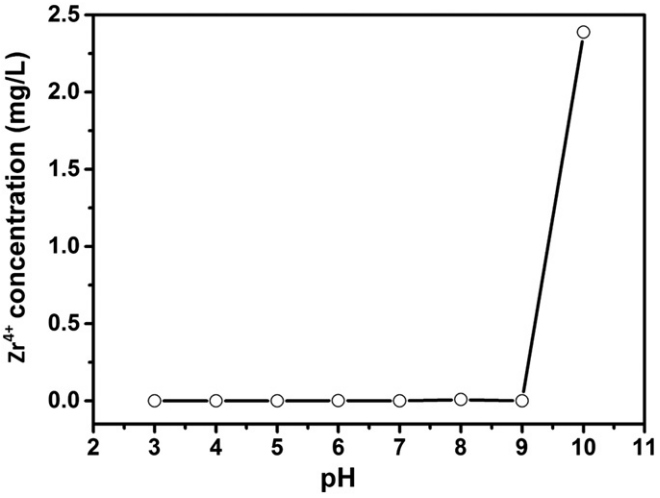

Fig. 9. The concentration of leaching Zr^{4+} ions in solution at various pHs by using Zr/Al-Mt.

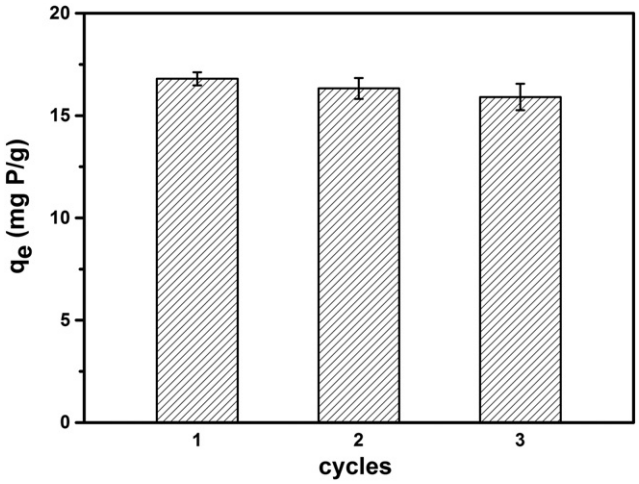

Fig. 10. Effect of adsorption-desorption cycles on the phosphate adsorption capacities of Zr/Al-Mt.

Acknowledgements

This work was supported by National Key Project in Control and Management of Polluted Water Bodies (No. 2013ZX07105-005), Natural Science Foundation of Guangdong (No. S2011040001667), the Fundamental Research Funds for the Central Universities (No. 21611310), Excellent Supervisor Program and the Zhejiang Province National Science Foundation (No. LQ14B070005). Ms Weiya Huang's study was supported by the program of China Scholarship Council (No. 201206780010).

References

Awual, M.R., Jyo, A., Ihara, T., Seko, N., Tamada, M., Lim, K.T., 2011. Enhanced trace phosphate removal from water by zirconium(IV) loaded fibrous adsorbent. Water Res. 45, 4592–4600.
Babel, S., Kurniawan, T., 2003. Low-cost adsorbents for heavy metals uptake from contaminated water: a review. J. Hazard. Mater. B97, 219–243.
Biswas, B.K., Inoue, K., Ghimire, K.N., Harada, H., Ohto, K., Kawakita, H., 2008. Removal and recovery of phosphorus from water by means of adsorption onto orange waste gel loaded with zirconium. Bioresour. Technol. 99, 8685–8690.
Cheung, C.W., Porter, J.F., McKay, G., 2001. Sorption kinetic analysis for the removal of cadmium ions from effluents using bone char. Water Res. 35, 605–612.
Chitrakar, R., Tezuka, S., Sonoda, A., Sakane, K., Ooi, K., Hirotsu, T., 2006. Selective adsorption of phosphate from seawater and wastewater by amorphous zirconium hydroxide. J. Colloid Interface Sci. 297, 426–433.
de Bashan, L.E., Bashan, Y., 2004. Recent advances in removing phosphorus from wastewater and its future use as fertilizer. Water Res. 38, 4222–4246.
Freundlich, H., 1906. Über die Adsorption in Lösungen. Universität Leipzig, Leipzig.

Genz, A., Kornmuller, A., Jekel, M., 2004. Advanced phosphorus removal from membrane filtrates by adsorption on activated aluminium oxide and granulated ferric hydroxide. Water Res. 38, 3523–3530.
Gil, A., Assis, F.C.C., Albeniz, S., Korili, S.A., 2011. Removal of dyes from wastewaters by adsorption on pillared clays. Chem. Eng. J. 168, 1032–1040.
Gimenez, J., Martinez, M., de Pablo, J., Rovira, M., Duro, L., 2007. Arsenic sorption onto natural hematite, magnetite, and goethite. J. Hazard. Mater. 141, 575–580.
Goldberg, S., Sposito, G., 1985. On the mechanism of specific phosphate adsorption by hydroxylated mineral surfaces: A review. Commun. Soil Sci. Plant Anal. 16, 801–821.
Grzmil, B., Wronkowski, J., 2006. Removal of phosphates and fluorides from industrial wastewater. Desalination 189, 261–268.
Guerra, D.L., Airoldi, C., Lemos, V.P., Angelica, R.S., 2008. Adsorptive, thermodynamic and kinetic performances of Al/Ti and Zr/Al-pillared clays from the Brazilian Amazon region for zinc cation removal. J. Hazard. Mater. 155, 230–242.
Haghseresht, F., Wang, S., Do, D.D., 2009. A novel lanthanum-modified bentonite, Phoslock, for phosphate removal from wastewaters. Appl. Clay Sci. 46, 369–375.
Ho, Y.S., 2006. Review of second-order models for adsorption systems. J. Hazard. Mater. 136, 681–689.
Ho, Y.S., Chiu, W.T., Hsu, C.S., Huang, C.T., 2004. Sorption of lead ions from aqueous solution using tree fern as a sorbent. Hydrometallurgy 73, 55–61.
Huang, W., Wang, S., Zhu, Z., Li, L., Yao, X., Rudolph, V., Haghseresht, F., 2008. Phosphate removal from wastewater using red mud. J. Hazard. Mater. 158, 35–42.
Kasama, T., Watanabe, Y., Yamada, H., Murakami, T., 2004. Sorption of phosphates on Al-pillared smectites and mica at acidic to neutral pH. Appl. Clay Sci. 25, 167–177.
Khan, A.A., Singh, R.P., 1987. Adsorption thermodynamics of carbofuran on Sn (IV) arsenosilicate in H^+, Na^+ and Ca^{2+} forms. Colloids Surf. 24, 33–42.
Koilraj, P., Kannan, S., 2010. Phosphate uptake behavior of ZnAlZr ternary layered double hydroxides through surface precipitation. J. Colloid Interface Sci. 341, 289–297.
Lagergren, S., 1898. Zur theorie der sogenannten adsorption gelöster stoffe. K. Svenska Vetenskapsakad. Handl. 24, 1–39.
Langmuir, I., 1917. The constitution and fundamental properties of solids and liquids. Part II. Liquids. J. Am. Chem. Soc. 39, 1848–1906.
Li, H., Ru, J., Yin, W., Liu, X., Wang, J., Zhang, W., 2009. Removal of phosphate from polluted water by lanthanum doped vesuvianite. J. Hazard. Mater. 168, 326–330.
Liu, H., Sun, X., Yin, C., Hu, C., 2008. Removal of phosphate by mesoporous ZrO_2. J. Hazard. Mater. 151, 616–622.
Long, F., Gong, J.L., Zeng, G.M., Chen, L., Wang, X.Y., Deng, J.H., Niu, Q.Y., Zhang, H.Y., Zhang, X.R., 2011. Removal of phosphate from aqueous solution by magnetic Fe-Zr binary oxide. Chem. Eng. J. 171, 448–455.
Ma, J., Qi, J., Yao, C., Cui, B., Zhang, T., Li, D., 2012. A novel bentonite-based adsorbent for anionic pollutant removal from water. Chem. Eng. J. 200–202, 97–103.
Morse, G.K., Brett, S.W., Guy, J.A., Lester, J.N., 1998. Review: Phosphorus removal and recovery technologies. Sci. Total Environ. 212, 69–81.
Mustafa, S., Zaman, M.I., Khan, S., 2006. pH effect on phosphate sorption by crystalline MnO_2. J. Colloid Interface Sci. 301, 370–375.
Na, P., Jia, X., Yuan, B., Li, Y., Na, J., Chen, Y., Wang, L., 2010. Arsenic adsorption on Ti-pillared montmorillonite. J. Chem. Technol. Biotechnol. 85, 708–714.
Namasivayam, C., Prathap, K., 2005. Recycling Fe(III)/Cr(III) hydroxide, an industrial solid waste for the removal of phosphate from water. J. Hazard. Mater. 123, 127–134.
Perrin, D.D., Dempsey, B., 1979. Buffers for pH and metal ion control. John Wiley & Sons, Inc., New York.
Prasad, M., Saxena, S., Amritphale, S.S., Chandra, N., 2000. Kinetics and Isotherms for Aqueous Lead Adsorption by Natural Minerals. Ind. Eng. Chem. Res. 39, 3034–3037.
Ren, Z., Zhang, G., Chen, J.P., 2011. Adsorptive removal of arsenic from water by an iron-zirconium binary oxide adsorbent. J. Colloid Interface Sci. 358, 230–237.
Ren, Z., Shao, L., Zhang, G., 2012. Adsorption of phosphate from aqueous solution using an iron-zirconium binary oxide sorbent. Water Air Soil Pollut. 223, 4221–4231.
Rodrigues, L., Maschio, L., Coppio, L., Thim, G., da Silva, M., 2012. Adsorption of phosphate from aqueous solution by hydrous zirconium oxide. Environ. Technol. 33, 1345–1351.
Tanada, S., Kabayama, M., Kawasaki, N., Sakiyama, T., Nakamura, T., Araki, M., 2003. Removal of phosphate by aluminum oxide hydroxide. J. Colloid Interface Sci. 257, 135–140.
Tian, S., Jiang, P., Ning, P., Su, Y., 2009. Enhanced adsorption removal of phosphate from water by mixed lanthanum/aluminum pillared montmorillonite. Chem. Eng. J. 151, 141–148.
Toranzo, R., Vicente, M.A., Bañares-Muñoz, M.A., Gandıa, L.M., Gil, A., 1998. Pillaring of saponite with zirconium oligomers. Microporous Mesoporous Mater. 24, 173–188.
Yan, L.g., Xu, Y.Y., Yu, H.Q., Xin, X.D., Wei, Q., Du, B., 2010. Adsorption of phosphate from aqueous solution by hydroxy-aluminum, hydroxy-iron and hydroxy-iron–aluminum pillared bentonites. J. Hazard. Mater. 179, 244–250.
Ye, H., Chen, F., Sheng, Y., Sheng, G., Fu, J., 2006. Adsorption of phosphate from aqueous solution onto modified palygorskites. Sep. Purif. Technol. 50, 283–290.
Zhang, Q., Du, Q., Jiao, T., Pan, B., Zhang, Z., Sun, Q., Wang, S., Wang, T., Gao, F., 2013. Selective removal of phosphate in waters using a novel of cation adsorbent: Zirconium phosphate (ZrP) behavior and mechanism. Chem. Eng. J. 221, 315–321.
Zhou, J., Wu, P., Dang, Z., Zhu, N., Li, P., Wu, J., Wang, X., 2010. Polymeric Fe/Zr pillared montmorillonite for the removal of Cr(VI) from aqueous solutions. Chem. Eng. J. 162, 1035–1044.
Zhou, Q., Wang, X.Z., Liu, J.Y., Zhang, L., 2012. Phosphorus removal from wastewater using nano-particulates of hydrated ferric oxide doped activated carbon fiber prepared by Sol-Gel method. Chem. Eng. J. 200, 619–626.